ELSEVIER

Contents lists available at ScienceDirect

Colloid and Interface Science Communications

journal homepage: www.elsevier.com/locate/colcom





Behavior of water confined between hydrophobic surfaces with grafted segments

Ramin Mehrani^a, Sumit Sharma^{b,*}

- a Department of Mechanical Engineering, Ohio University, Athens, OH 45701, United States
- b Department of Chemical and Biomolecular Engineering, Ohio University, Athens, OH 45701, United States

ABSTRACT

Many naturally occurring as well as functionalized interfaces are covered with protruding segments or side-chain moieties. These protruding segments influence interfacial properties, and play an important role in diverse physical processes that are understood to be driven by water-mediated interactions, ranging from protein folding, protein dimerization to nanoparticle self-assembly in aqueous media. We have studied the behavior of water confined between two planar hydrophobic surfaces with grafted segments using molecular simulations. We show the presence of these segments makes the confined region significantly more hydrophobic. By systematically varying the flexibility of these segments over a range spanning two orders of magnitude for two different grafting densities, we report that the flexibility of the segments itself has no effect on the free energy profile of confined water. We also find that the evaporation free energy barrier increases and the condensation free energy barrier decreases as the density of the grafted segment is increased.

1. Introduction

Water-mediated interactions are known to play an important role in many processes, such as self-assembly of lipid bilayers [5,33,36], folding of globular proteins [19,27] as well as in the manifestation of complex rheology of suspensions [16]. The behavior of water near hydrophobic solutes has an interesting length-scale dependence. Near small hydrophobic solutes (< 1 nm) that are incapable of forming hydrogen bonds, water molecules retain their hydrogen bonds by forming a network around them. This results in an entropic penalty associated with the dissolution of small hydrophobic solutes in water [31]. Near a large hydrophobic solute (> 1 nm), water molecules are unable to retain all their hydrogen bonds, which leads to an enthalpic penalty for the dissolution of large hydrophobic solutes in water [5,32]. Due to lack of hydrogen bonding, the region close to a large hydrophobic solute is akin to a vapor-liquid interface, which manifests large density fluctuations. Thermodynamic considerations suggest that liquid water confined between two large hydrophobic surfaces becomes meta-stable with respect to the vapor phase below some critical confinement gap [22,29]. This critical gap for nanoscopic solutes is of O(nm) [4,12], but becomes as much as $O(\mu m)$ for macroscopic solutes. Though thermodynamically the vapor phase is more stable below the critical confinement gap, there is a free energy barrier associated with the evaporation of confined liquid water, which has been shown to increase remarkably with the confinement gap [25,29]. Therefore, metastable liquid water may persist under hydrophobic confinement for long time durations [28].

So far, studies have mainly focused on investigating the behavior of confined water between two smooth hydrophobic surfaces, with some notable exceptions [9,10,26]. However, in many physical systems of interest, confining surfaces have protruding segments, which may significantly impact the behavior of confined water. For instance, in α -helical secondary structures of proteins, the side chains protrude outwards. During the packing of these α -helices in tertiary structures like helix bundles, the effect of the protruding side chains is understood to be important as the side chains influence the behavior of water in the confined region between the helices [6]. Similarly, during the dimerization of proteins, large ($\approx 1500-3000 \text{ Å}$) and relatively flat protein interfaces come in close proximity, and the exposed side chains of the amino acids at the binding interface are likely to affect the stability of water in the confined region [7,11]. Furthermore, adsorbed surfactant molecules on metal nanoparticles result in nanoparticle surfaces with protruding alkyl tails that have been shown to facilitate nanoparticle self-assembly in ordered two- and three-dimensional structures, useful for applications like nanofabrication [15,35]. Therefore, understanding the effect of segments protruding out of surfaces on the stability of confined water is quite important. Recently, Debenedetti and coworkers have demonstrated, using theory and molecular simulations, that the free energy barrier to evaporation decreases dramatically as the confining surfaces become increasingly flexible due to the additional contribution coming from the energy of deformation of the surfaces

E-mail address: sharmas@ohio.edu (S. Sharma).

^{*} Corresponding author.

[1,2]. The dependence of the free energy barrier on the flexibility of surfaces makes one contemplate if the presence of flexible segments grafted onto the surfaces will have an analogous effect. In this work, we explore this question by determining the free energy profiles of water confined between two hydrophobic surfaces with grafted segments of different flexibility.

1.1. Simulation system and methods

The simulation system comprises of two parallel hydrophobic surfaces submerged in water. Each surface is made up of 896 atoms arranged in a hexagonal lattice with a lattice constant of 1.4 Å. Lateral dimensions of the surfaces are 37.584 \times 38.5 Å². Fig. 1 shows set-up of the simulation system. Flexible segments are grafted on the face of the surfaces that are toward the confined region. Each segment is made up of three atoms connected to each other via harmonic bonds of equilibrium length of 1.4 Å. Adjacent bonds within the segments have a harmonic angular potential with the equilibrium angle of 180° between them. In addition, the flexible segments are kept perpendicular to the surfaces via two harmonic angular potentials with the equilibrium angle of 90°. These two angular potentials are between the bond joining the lowermost atom of the segment to the surface atom at the point of attachment, and the bond between the atom of attachment and an adjacent atom on the surface. We have studied two different grafting densities: 0.0387 segments/Å² and 0.1548 segments/Å² as shown in Fig. 2, henceforth referred to as low-density and high-density respectively. Grafting density is defined as the number of segments per unit area of the surface.

Distance between the surfaces, d is kept fixed at 25 Å and consequently the center-to-center distance between the terminal atoms of the segments on opposite surfaces is nominally 16.6 Å. Distance between the surfaces is defined as the center-to-center distance between the lattice planes of the atoms that comprise the two surfaces. The simulation box size is $70 \times 70 \times 70$ ų. The simulation system contains 11,325 water molecules. Water molecules are modeled as simple point charge enhanced (SPC/E, a three-site, rigid water model) [3]. The interactions between the surfaces and the segment atoms are set to zero. Interactions between the segment atoms are also set to zero. The surface and the

segment atoms interact with the oxygen of water molecules via Lennard-Jones potential with parameters of $\varepsilon = 0.0289$ *kcal/mol* and $\sigma = 3.28$ Å, as in our previous studies [29]. The k-space part of Coulombic interactions is calculated via Particle-Particle Particle-Mesh Ewald. Flexibility of the segments is changed by modifying the angle and bond force constants, k_{θ} and k_{r} , associated with the harmonic potentials. Free energy profiles of confined water are calculated by implementing indirect umbrella sampling (INDUS) in molecular dynamics (MD) [23,24,34]. INDUS is an umbrella sampling methodology wherein the bias potential is a harmonic function of the number of molecules inside a probe volume. The bias potential is given by $U_{Bias} = \kappa (N - N_0)^2$, where N is the number of molecules in the probe volume; N_0 is the set-value of N for a sampling window; and κ is the pre-factor of the biased harmonic potential. By systematically varying N_0 from 0 to N_{liq} (N_{liq} is the equilibrium number of water molecules in the confined region in the liquid state) all intermediate values of N are sampled. In the INDUS implementation, the density of particles is smeared in space by modeling it as a truncated Gaussian distribution centered at the location of each particle [23,24]. The cutoff length and the standard deviation of the Gaussian function are set to 0.3 Å and 0.1 Å respectively while the κ value is set to 0.1 kcal/mol. From the umbrella sampling windows thus generated, unbiased free energy profiles are obtained by applying the Weighted Histogram Analysis Method (WHAM) [13,18,21,30].

We have performed INDUS [23,24] simulations in the isothermalisobaric (NPT) ensemble at the pressure and temperature of 1 bar and 298 K. In the simulations, the initial configuration is equilibrated for 1 ns , which is followed by a production run of 15 ns for the low-density and 23 ns for the high-density system. The time step used in the simulations is 1 femtosecond (fs). To study the effect of flexibility of the segments, free energy profiles of confined water are calculated by varying the values of the bond and the angular harmonic potential coefficients, k_{θ} and k_r from 50 to 1000 Kcal/mole-Ų and 50 to 1000 Kcal/mole – rad² respectively. For each estimate of the free energy profile, N_0 is varied from 0 to 650 in increments of 5, which results in 131 INDUS windows. We have employed two independent Nose'-Hoover thermostats, one for the flexible segments and one for the water molecules to prevent unequal distribution of kinetic energies between the degrees of

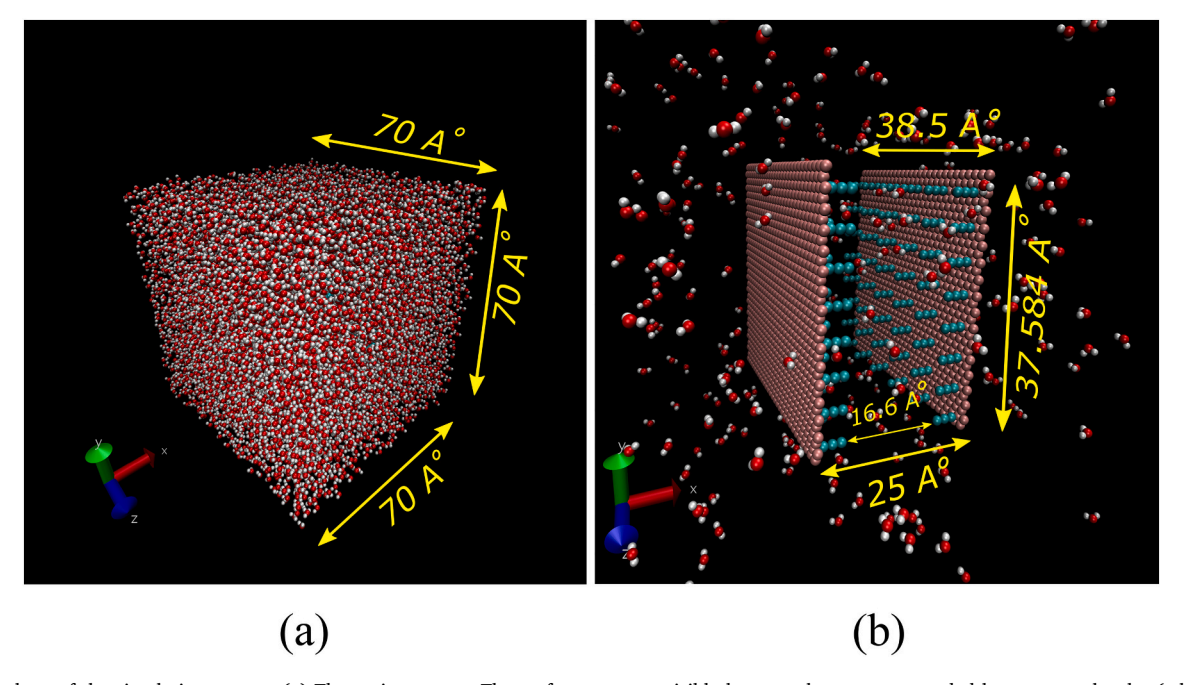


Fig. 1. Snapshots of the simulation system: (a) The entire system. The surfaces are not visible because they are surrounded by water molecules (white and red represent hydrogen and oxygen atoms of water respectively). (b) The two hydrophobic surfaces with grafted segments. Most water molecules have been removed for the purpose of showing the surfaces and the segments. (For interpretation of the references to colour in this figure legend, the reader is referred to the web version of this article.)

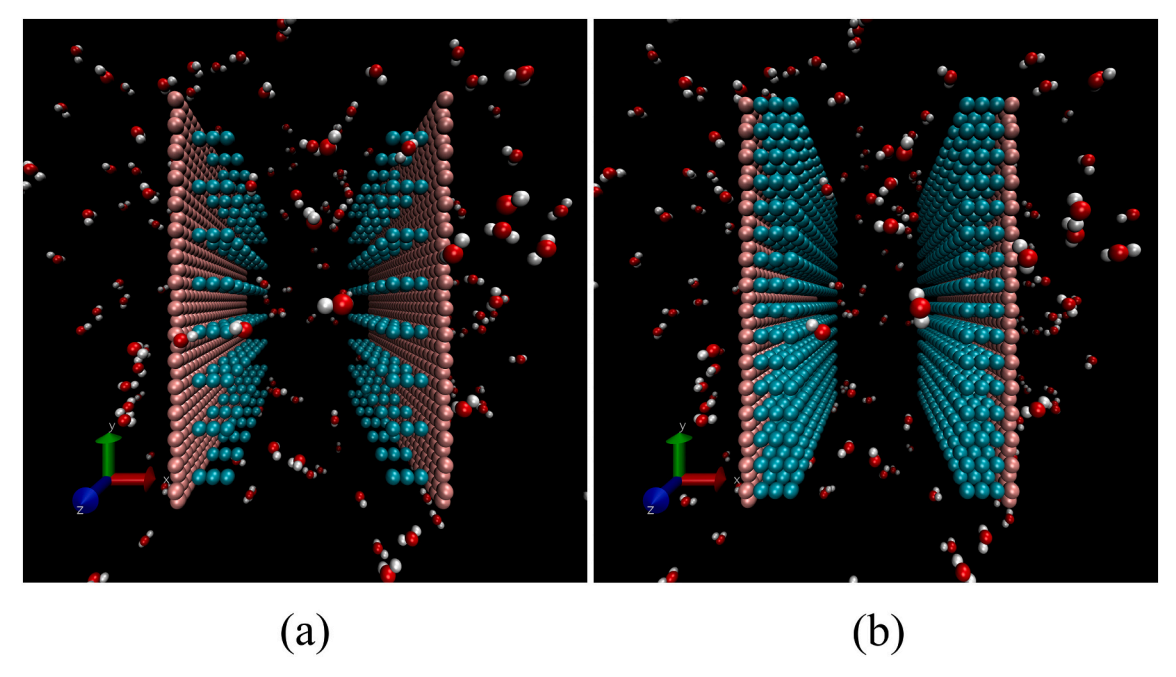


Fig. 2. Hydrophobic surfaces with grafted flexible segments at two different grafting densities: (a) 0.0387 segment/Å², and (b) 0.1548 segment/Å².

freedom of the flexible segments and the solvent, which is referred to as the flying ice-cube problem [14].

2. Results and discussion

Fig. 3 shows density profiles of water in the presence and absence of grafted segments. In the absence of the flexible segments, the confined region shows layering of water molecules parallel to the surfaces. Whereas, in the presence of the flexible segments, the layering disappears for both the segment densities. It is understood that the presence of flexible segments makes the surfaces more hydrophobic, and therefore one would expect to see the layering of water in the confined region to become less prominent as compared to the system without the segments

[20]. Even for the smaller grafting density of $0.0387\ chain/\text{Å}^2$, water molecules are unable to enter the inter-segment region, as the distance between the segments within a surface is from $2.4-2.8\ \text{Å}$. Furthermore, it is observed that the density profiles of confined water do not depend on the flexibility of the segments. Kanduc et al. [17] have studied the effect of flexibility of the molecules of self-assembled monolayers (SAMs) on confined water and have shown that increasing the flexibility decreases the layering of confined water, which is related to significant changes in the pressure of the system. In our study, the surfaces are of finite size and the pressure is kept constant. Dallin and Van Lehn [8] have shown that disordered SAM configurations permit penetration of water molecules into the alkanethiol SAM that decreases the surface hydrophobicity. In our system, we did not observe any significant

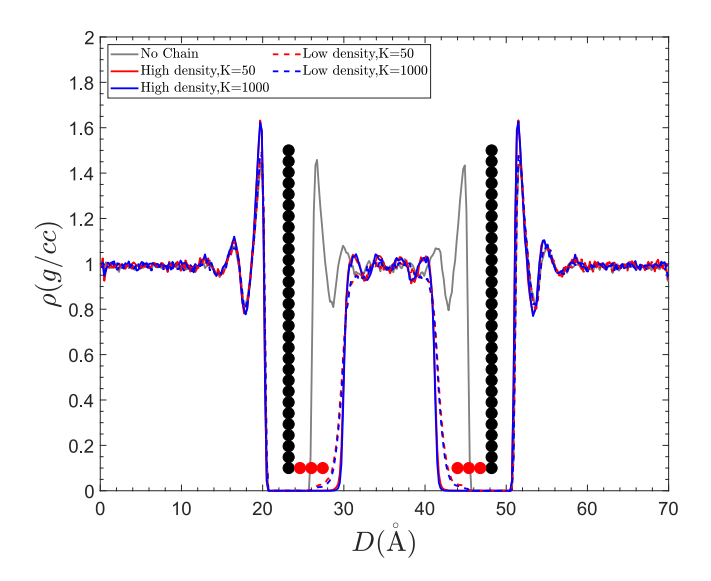


Fig. 3. Density profile of water confined between two hydrophobic surfaces in the presence and absence of grafted flexible segments. The black and the red circles represent the surfaces and the flexible segments respectively. The legend shows the values of the k_θ and the k_r . High values of k_θ and k_r correspond to low flexibility of the segments. (For interpretation of the references to colour in this figure legend, the reader is referred to the web version of this article.)

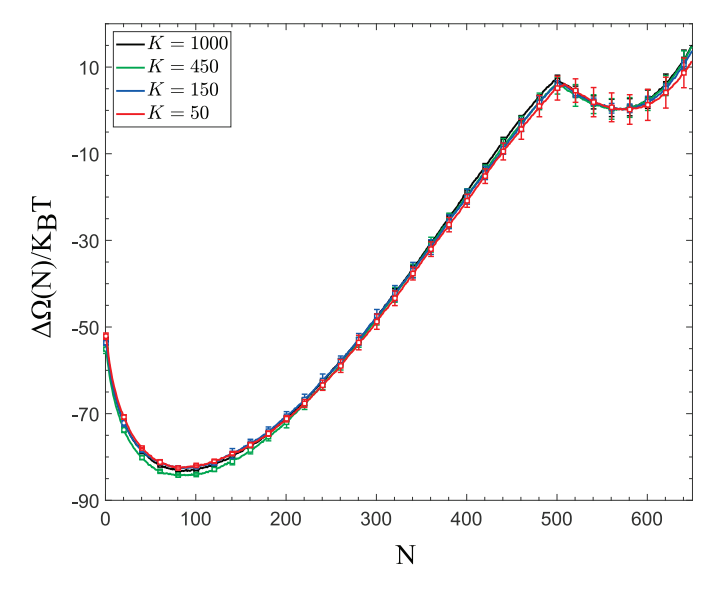


Fig. 4. Free energy profiles, $\Delta\Omega(N)$, of confined water as a function of the flexibility of grafted segments with the grafted density of 0.0387 *chain*/Å². Error bars are standard deviations obtained from four independent simulations. The numbers in the legend show the values of k_θ and k_r . $\Delta\Omega(N)$ are found to be invariant of the flexibility of the segments.

changes in the penetration of the water molecules between the segments as a function of the flexibility of the segments. Fig. 4 shows free energy profiles, $\Delta\Omega(N)$, of water confined between the surfaces with flexible segments as a function of their flexibility, for the case of low grafting density. Flexibility of the segments is varied by changing the values of k_{θ} and k_r from 50 to 1000 Kcal/mole-Å² and 50 to 1000 Kcal/mole – rad² respectively. We find that the free energy barrier to evaporation of water is $\approx 6K_BT$. As expected, this free energy barrier is much smaller than the barrier of 23 K_BT that is obtained when the surfaces do not have any grafted flexible segments [25]. Interestingly, the $\Delta\Omega(N)$ obtained for the different segment flexibilities overlap, which implies that the flexibility of the segments does not impact the free energy behavior of water. Fig. 5 shows the $\Delta\Omega(N)$ for the grafting density of 0.1548 segment/Å², that is, the high-density case. Even with an increase in the segment density by a factor of almost 3, the liquid phase is still found to be meta-stable with respect to the vapor phase. The free energy barrier to evaporation is \approx $14k_BT$. Interestingly, for the higher-density case as well, we find the $\Delta\Omega(N)$ of water to be independent on the flexibility of the segments. This result confirms the conclusion that the flexibility of the grafted segments does not affect the free energy behavior of confined water, even though the flexibilities are varied by two orders of magnitude. To confirm that the invariance of the $\Delta\Omega(N)$ is not an artifact of the projection of the free energy on the order parameter, N, we have calculated the free energy profiles along a second order parameter, the radius of the vapor tube, R. Since it has been established that the evaporation of water occurs via formation of a vapor tube in the confined region, the R is a logical order parameter [25,28,29]. The probability of finding a configuration with R $=R_o$ is given by: $P(R_o)=\int_{\widetilde{N}}P\Big(\widetilde{N}\Big)h\Big(R_o|\widetilde{N}\Big)d\widetilde{N}.$ In this expression, \widetilde{N} represents the number of water molecules in the confined region when the density is considered smeared in space via Gaussian distributions. That is, $\widetilde{N} \in IR$. $h(R_0|\widetilde{N})$ is the probability of finding a value of R_0 for a given \widetilde{N} . The radius of the vapor tube in a configuration, R is calculated by projecting all the confined water molecules on to the x-y plane of the surface. The plane is divided into square grids of size $0.2 \times 0.2 \text{ Å}^2$. Each cell is then labeled as "occupied" or "vacant" depending on whether the center of the cell is within a distance of 1.583 Å from the projection of any water molecule. Largest 2D cluster of vacant cells is then identified by performing a cluster analysis on the vacant cells. R is estimated by

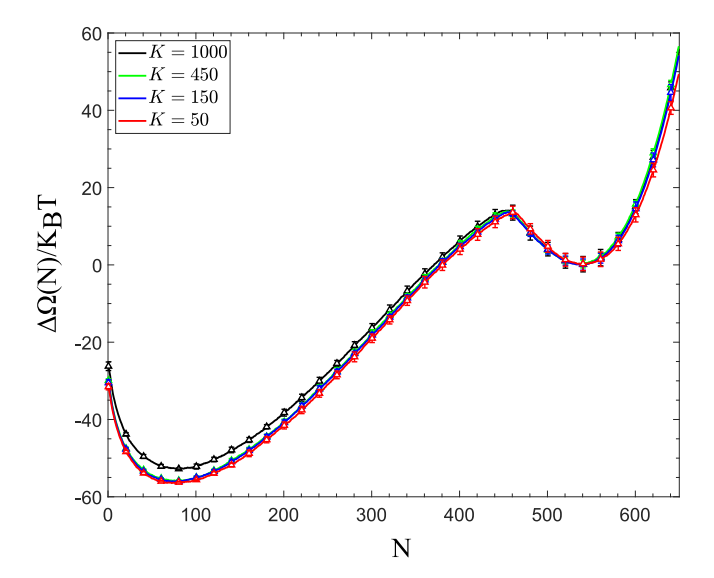


Fig. 5. Free energy profiles, $\Delta\Omega(N)$, of confined water as a function of number of the confined water molecules at different flexibilities of grafted segments with the grafted density of 0.1548 *chain*/Ų. Error bars are standard deviations obtained from three independent simulations. The numbers in the legend show the values of k_θ and k_r .

assuming the largest cluster to be a circle. This procedure of finding R has been employed in a previous publication [29]. The free energy profile as a function of R is obtained by $\Delta\Omega(R) = -k_BT \ln{(P(R))}$. The value of R for different configurations as a function of N is shown in the fig. S1 (Supporting Information). The free energy profile as a function of R is plotted in the Fig. 6 for systems with flexible segments of varying flexibilities for both the low- and high-density cases. Comparison of the free energy of confined water for the two segment densities shows that increasing the segment density decreases the condensation free energy barrier and increases the evaporation free energy barrier. Also, the free energy profiles, $\Delta\Omega(R)$ are found to be invariant of the segment flexibility. This result corroborates with the finding that the free energy profiles of confined water are unaffected by the flexibility of grafted segments. The $\Delta\Omega(R)$ show a broad peak, which implies that the configurations with a range of R values form the maximum in the free energy profiles. In order to understand the lack of dependence of the free energy profiles on the flexibility of the segments, we have plotted ensemble-averaged total harmonic potential, $U_{\theta} + U_{r}$ of all the segments as a function of N for the two grafted densities in the Figs. 7 and 8. The figures show that there is no systematic change in the $U_{\theta} + U_{r}$ as a function of N for both the grafting densities. This result shows that the elastic energy of the segments does not change as the N changes, and therefore verifies the conclusion that the flexibility of the segments does not affect the free energy profiles of confined water. Finally, we have calculated the $\Delta\Omega(N)$ of confined water in a system devoid of any flexible segments (Figs. S2 and S3, Supporting Information). In this system, two surfaces are placed parallel to each other and at a d of 16.6 Å. On these surfaces, the atoms on which the flexible segments were attached in the case of high grafting density (Fig. 2(b)) interact with water-oxygen via the LJ potential with the parameters same as for the segments. The other atoms on these surfaces interact with water-oxygen with the purely repulsive Week-Chandler-Andersen (WCA) potential. Therefore, these surfaces that are decorated with LJ atoms mimic the kind of interactions that an interface with flexible segments will present. In addition, we place another set of surfaces parallel to each other and to the above surfaces, at a distance of d of 25 Å. Kindly see the Fig. S2 (Supporting Information) for the system configuration. These outer surfaces interact with water-oxygen via the LJ potential with the same parameters as the case with the flexible segments. So, in this system, we

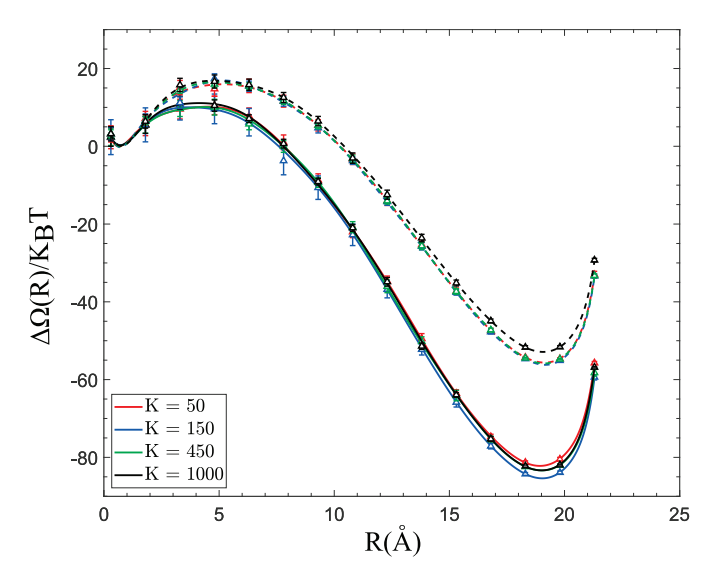


Fig. 6. Free energy profiles, $\Delta\Omega(R)$ of confined water as a function of radius of the vapor tube, $\Delta\Omega(R)$ for different flexibilities of grafted segments. The solid lines represent the low grafting density of 0.0387 *chain*/Ų and the dashed lines represent the high grafting density of 0.1548 *chain*/Ų. Error bars are standard deviations obtained from independent simulations. The numbers in the legend show the values of k_{θ} and k_{r} .

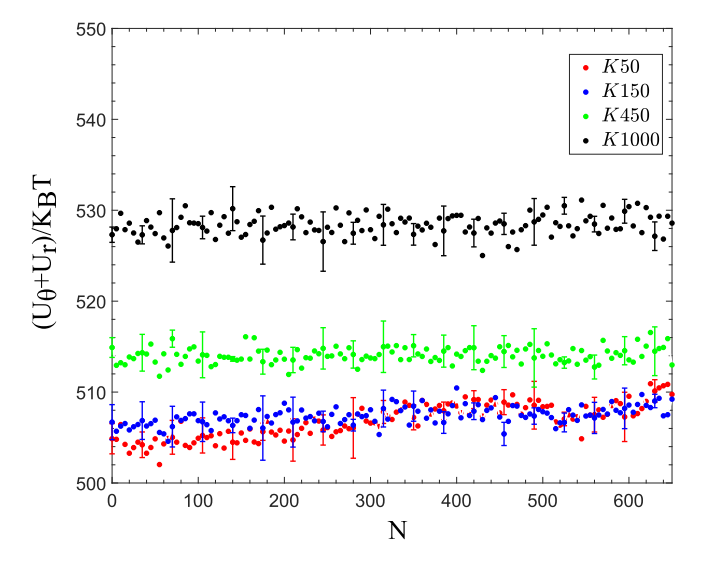


Fig. 7. Ensemble-averaged total harmonic potential as a function of N for different segments' flexibilities at low grafted density. The numbers in legend show the value of the k_{θ} and k_r and the error bars are standard deviation calculated from four different simulations.

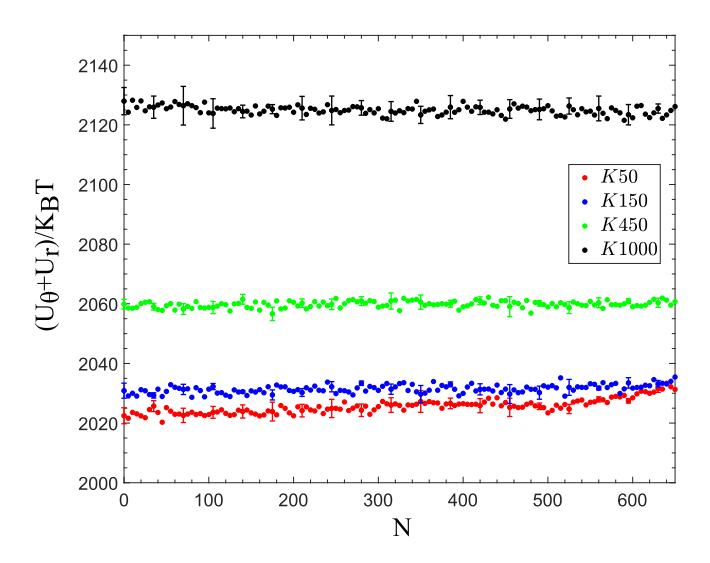


Fig. 8. Ensemble-averaged total harmonic potential as function of N for different segments' flexibilities at high grafted density. The numbers in legend show the value of the k_{θ} and k_r and the error bars are standard deviation calculated from four different simulations.

have attempted to closely mimic the system with high density of grafted segments, but in the absence of the segments. The $\Delta\Omega(N)$ for this system is shown in Fig. S3 (Supporting Information). The $\Delta\Omega(N)$ of this system is remarkably different from the case with the flexible segments. First, there is no free energy barrier to evaporation, implying that the liquidwater is no longer meta-stable, but is unstable. In addition, the free energy barrier to condensation in this case is $\approx 170k_BT$, whereas it is $\approx 60k_BT$ for the case of flexible segments. This result shows that the behavior of water when confined between two surfaces with grafted flexible segments cannot simply be explained by the loss of attractive interactions of water-oxygen with the surface atoms. An explanation of the difference between the profiles with and without the segments will be that due to the presence of WCA atoms, the confinement effect is enhanced.

3. Conclusions

We have studied the effect of the presence of grafted flexible segments at two different grafted densities and for a range of segments' flexibilities on the free energy profiles of confined water. We find that the surfaces with grafted flexible segments are highly hydrophobic, thus rendering liquid water in the confined region to be meta-stable with respect to the vapor phase. Furthermore, we show that the flexibility of the segments has no perceivable effect on the free energy profiles of confined water. The invariance of the free energy profiles as a function of segment flexibility eliminates a large parameter space that otherwise would need to be explored in order to understand the behavior of the water confined between two surfaces with grafted flexible segments. This result is in contrast to the previous observations that the flexibility of the confining surfaces has a significant effect on the free energy profile of confined water [1,2]. Unlike in the case of flexible surfaces, no change is observed in the elastic potential energy of the flexible segments as a function of the number of confined water molecules.

Author statement

Ramin Mehrani: Methodology, Software, Validation, Formal Analysis, Writing – Original Draft, Investigation, Visualization. Sumit Sharma: Conceptualization, Methodology, Writing – Review & Editing, Supervision, Project administration, Funding acquisition.

Declaration of Competing Interest

The authors declare that they have no known competing financial interests or personal relationships that could have appeared to influence the work reported in this paper.

Acknowledgments

This work is supported by the National Science Foundation CDS&E grant 1953311. Computational resources for this work were provided by the Ohio Supercomputer Center and National Science Foundation XSEDE grant number DMR190005.

Appendix A. Supplementary data

Supplementary data to this article can be found online at $\frac{\text{https:}}{\text{doi.}}$ org/10.1016/j.colcom.2020.100355.

References

- Y.E. Altabet, P.G. Debenedetti, The role of material flexibility on the drying transition of water between hydrophobic objects: a thermodynamic analysis, J. Chem. Phys. 141 (18) (2014) 18C531.
- [2] Y.E. Altabet, A. Haji-Akbari, P.G. Debenedetti, Effect of material flexibility on the thermodynamics and kinetics of hydrophobically induced evaporation of water, Proc. Natl. Acad. Sci. 114 (13) (2017) E2548–E2555.
- [3] H. Berendsen, J. Grigera, T. Straatsma, The missing term in effective pair potentials, J. Phys. Chem. 91 (24) (1987) 6269–6271.
- [4] C.A. Cerdeiriña, P.G. Debenedetti, P.J. Rossky, N. Giovambattista, Evaporation length scales of confined water and some common organic liquids, J. Phys. Chem. Lett. 2 (9) (2011) 1000–1003.
- [5] D. Chandler, Interfaces and the driving force of hydrophobic assembly, Nature 437 (7059) (2005) 640.
- [6] K.-C. Chou, C.-T. Zhang, G.M. Maggiora, Disposition of amphiphilic helices in heteropolar environments, Proteins: Structure, Function, and Bioinformatics 28 (1) (1997) 99–108.
- [7] T. Clackson, J.A. Wells, A hot spot of binding energy in a hormone-receptor interface, Science 267 (5196) (1995) 383–386.
- [8] B.C. Dallin, R.C. Van Lehn, Spatially heterogeneous water properties at disordered surfaces decrease the hydrophobicity of nonpolar self-assembled monolayers, J. Phys. Chem. Lett. 10 (14) (2019) 3991–3997.
- [9] B.C. Dallin, H. Yeon, A.R. Ostwalt, N.L. Abbott, R.C. Van Lehn, Molecular order affects interfacial water structure and temperature-dependent hydrophobic interactions between nonpolar self-assembled monolayers, Langmuir 35 (6) (2019) 2078–2088.

- [10] C.D. Daub, J. Wang, S. Kudesia, D. Bratko, A. Luzar, The influence of molecularscale roughness on the surface spreading of an aqueous nanodrop, Faraday Discuss. 146 (2010) 67–77.
- [11] S. Eyrisch, V. Helms, Transient pockets on protein surfaces involved in proteinprotein interaction, J. Med. Chem. 50 (15) (2007) 3457–3464.
- [12] M. Ghasemi, S.M. Ramsheh, S. Sharma, Quantitative assessment of thermodynamic theory in elucidating the behavior of water under hydrophobic confinement, J. Phys. Chem. B 122 (50) (2018) 12087–12096.
- [13] Grossfield, A. Wham: the weighted histogram analysis method. WHAM: the weighted histogram analysis method, Version 2.0.9.
- [14] S.C. Harvey, R.K.-Z. Tan, T.E. Cheatham III, The flying ice cube: velocity rescaling in molecular dynamics leads to violation of energy equipartition, J. Comput. Chem. 19 (7) (1998) 726–740.
- [15] X. Huang, I.H. El-Sayed, W. Qian, M.A. El-Sayed, Cancer cell imaging and photothermal therapy in the near-infrared region by using gold nanorods, J. Am. Chem. Soc. 128 (6) (2006) 2115–2120.
- [16] N.M. James, E. Han, R.A.L. de la Cruz, J. Jureller, H.M. Jaeger, Interparticle hydrogen bonding can elicit shear jamming in dense suspensions, Nat. Mater. 17 (11) (2018) 965.
- [17] M. Kanduc, A. Schlaich, E. Schneck, R.R. Netz, Water-mediated interactions between hydrophilic and hydrophobic surfaces, Langmuir 32 (35) (2016) 2027, 2029.
- [18] J. Kästner, Umbrella sampling, Wiley Interdisciplinary Reviews: Computational Molecular Science 1 (6) (2011) 932–942.
- [19] W. Kauzmann, Some factors in the interpretation of protein denaturation, in: Advances in Protein Chemistry volume 14, Elsevier, 1959, pp. 1–63.
- [20] P. Kumar, F.W. Starr, S.V. Buldyrev, H.E. Stanley, Effect of water-wall interaction potential on the properties of nanoconfined water, Phys. Rev. E 75 (1) (2007), 011202
- [21] S. Kumar, J.M. Rosenberg, D. Bouzida, R.H. Swendsen, P.A. Kollman, The weighted histogram analysis method for free-energy calculations on biomolecules. i. the method, J. Comput. Chem. 13 (8) (1992) 1011–1021.
- [22] K. Lum, D. Chandler, J.D. Weeks, Hydrophobicity at small and large length scales, J. Phys. Chem. B 103 (22) (1999) 4570-4577.

- [23] A.J. Patel, P. Varilly, D. Chandler, Fluctuations of water near extended hydrophobic and hydrophilic surfaces, J. Phys. Chem. B 114 (4) (2010) 1632–1637.
- [24] A.J. Patel, P. Varilly, D. Chandler, S. Garde, Quantifying density fluctuations in volumes of all shapes and sizes using indirect umbrella sampling, J. Stat. Phys. 145 (2) (2011) 265–275.
- [25] R.C. Remsing, E. Xi, S. Vembanur, S. Sharma, P.G. Debenedetti, S. Garde, A. J. Patel, Pathways to dewetting in hydrophobic confinement, Proc. Natl. Acad. Sci. 112 (27) (2015) 8181–8186.
- [26] J.A. Ritchie, J.S. Yazdi, D. Bratko, A. Luzar, Metastable sessile nanodroplets on nanopatterned surfaces, J. Phys. Chem. C 116 (15) (2012) 8634–8641.
- [27] G.D. Rose, S. RoY, Hydrophobic basis of packing in globular proteins, Proc. Natl. Acad. Sci. 77 (8) (1980) 4643–4647.
- [28] S. Sharma, P.G. Debenedetti, Evaporation rate of water in hydrophobic confinement, Proc. Natl. Acad. Sci. 109 (12) (2012) 4365–4370.
- [29] S. Sharma, P.G. Debenedetti, Free energy barriers to evaporation of water in hydrophobic confinement, J. Phys. Chem. B 116 (44) (2012) 13282–13289.
- [30] M. Souaille, B. Roux, Extension to the weighted histogram analysis method: combining umbrella sampling with free energy calculations, Comput. Phys. Commun. 135 (1) (2001) 40–57.
- [31] N.T. Southall, K.A. Dill, A. Haymet, A view of the hydrophobic effect, J. Phys. Chem. B 106 (3) (2002) 521–533.
- [32] F.H. Stillinger, Structure in aqueous solutions of nonpolar solutes from the standpoint of scaled-particle theory, in: The Physical Chemistry of Aqueous System, Springer, 1973, pp. 43–60.
- [33] C. Tanford, The Hydrophobic Effect: Formation of Micelles and Biological Membranes 2d Ed, J. Wiley, 1980.
- [34] G.M. Torrie, J.P. Valleau, Nonphysical sampling distributions in Monte Carlo freeenergy estimation: umbrella sampling, J. Comput. Phys. 23 (2) (1977) 187–199.
- [35] Y. Wang, A.E. DePrince III, S.K. Gray, X.-M. Lin, M. Pelton, Solvent-mediated end-to-end assembly of gold nanorods, J. Phys. Chem. Lett. 1 (18) (2010) 2692–2698.
- [36] W.C. Wimley, S.H. White, Membrane partitioning: distinguishing bilayer effects from the hydrophobic effect, Biochemistry 32 (25) (1993) 6307–6312.